Silicon (2022) 14:9643–9657
https://doi.org/10.1007/s12633-021-01631-1

ORIGINAL PAPER

Impact of elevated temperature over different properties of CVD SiCN coating developed in Nitrogen gas atmosphere

Soham Das[1] · Dhruva Kumar[1] · Rishikesh Borah[1] · Abhinov Dutta[1] · Spandan Guha[2]

Received: 16 October 2021 / Accepted: 16 December 2021 / Published online: 3 February 2022
© The Author(s), under exclusive licence to Springer Nature B.V. 2022

Abstract
Silicon carbonitride (SiCN) thin film has been deposited over the p-type c-Si (100) substrate by thermal chemical vapor deposition (CVD) process in the nitrogen (N_2) gas atmosphere under different deposition temperatures. The scanning electron microscopy (SEM) images have confirmed the presence of randomly distributed agglomerated particles of different sizes over the surface. The atomic force microscopy (AFM) analysis reveals consecutive reduction of particle size with higher deposition temperature whereas particle distribution density increases with higher temperature due to the increased randomness of gaseous molecules within the chamber. The x-ray diffraction (XRD) analysis reveals the presence of peaks at (110), (200), (201), (102) and (400) crystal planes with reduced crystallite size with higher temperatures. The Fourier transform infrared radiation (FTIR) analysis indicates the intensity of Si–N-Si functional group is higher compared to others due to the presence of higher nitrogen content in the film and these results are in good agreement with the results obtained from energy dispersive X-Ray spectroscopy (EDS) analysis. The Photoluminescence (PL) spectra analysis indicates that the blue shift of wavelength is a function of laser power. The estimation of mechanical properties reveals the maximum hardness (H) and Young's modulus (E) of SiCN coating are 27.89 and 302.30 GPa respectively obtained for the film deposited at 950 °C. The data analysis of SiCN thin film coating has been done by using Origin 9.0 software.

Keywords SiCN · CVD · Thin film coating · Structural property · Mechanical property

1 Introduction

The application of SiCN as well as polymer derived (PD) SiCN has attracted huge attention among various researchers due to their excellent electromagnetic characteristics, microwave absorption ability and excellent mechanical properties [1, 2]. It is paramount important to investigate the physical, tribological and mechanical properties of this alloy to achieve higher efficiency. Even it's vital to measure and analyse different characteristics of thin film coating at elevated temperature for the purpose of basic scientific investigation and practical field applications. Generally at the time of manufacturing, materials are exposed to higher temperature so it's difficult to measure these properties at room temperature level as part of the deformation is thermally activated e.g. hardness and yield stress of materials usually decreases due to excessive wear and thermal softening. The material which is to be used for different elevated temperature applications has to satisfy various specific chemical and physical properties e.g. corrosion resistance, high melting point, creep resistivity along with compositional and structural ability, sufficient strength at high temperature and acceptable oxidation etc. Even low density is also necessary for aerospace and transportation industry [3]. It has been observed that materials are exposed to elevated temperatures lead to thermal softening and higher wear rate due to consecutive reduction in hardness and yield stress [3]. The thin-film coating used for metal cutting purposes needs to reach up to a specific standard such as high melting point, good adhesion with the parent material, high hardness, compositional and structural stability etc. [3]. In this regard, ternary SiCN has been considered as one of the most attractive materials for the entire research community because

✉ Spandan Guha
spandan.guha@yahoo.com

1 Department of Mechanical Engineering, Sikkim Manipal Institute of Technology, Sikkim Manipal University, Majhitar, Rangpo-East Sikkim, India 737136

2 School of Mechanical Engineering, KIIT University, Bhubaneswar, India 751024

of its exceptional optical, tribological and mechanical properties along with considerable chemical inertness [3]. Based on molar composition, SiCN possesses excellent hardness [4], creep resistance and oxidation resistance up to a temperature range of 1600 °C [5, 6]. SiCN also exhibits a low coefficient of friction [7] with sound tribological and optical properties [8, 9]. The high chemical inertness and higher electrical conductivity of SiCN alloy make it a very popular alternative in microelectromechanical systems (MEMS) [10–13] and various other applications such as heat flux sensors, sensors used in turbines and high temperature/pressure transducers [14–17]. So far, the synthesis of SiCN has been carried out by many researchers for various applications. Peng et al. [18] investigated the effect of target voltage on the chemical composition and bonding of SiCN coated Silicon (Si) substrate synthesized by RF sputtering technique. They reported enhancement in bonding configuration and chemical composition with an appropriate adjustment of plasma energy used in the RF sputtering technique. Wrobel et al. [19] analyzed the physical properties of SiCN coating synthesized by the RP-CVD technique. Awad et al. [20] investigated the mechanical and structural properties of VT-CVD based SiCN coating. Badzian et al. [21] investigated the stability of microwave plasma CVD etched SiCN thin film in the nitrogenous surrounding. Kumar et al. [22] investigated the effect of N_2 flow rate on the mechanical properties of CVD SiCN coating. The authors reported enhancement in the mechanical properties of the SiCN coating with a higher N_2 flow rate. Swain et al. [23] reported an increase in carbon percentage with a consecutive decrease in Si of SiCN:H coating with an increased H_2 flow rate. Zhao et al. [24] used a high frequency- CVD (HFCVD) technique to deposit SiCN on Si substrate and found SiCN coating with sharp-featured particles. Bachar et al. [25] successfully synthesized SiCN film using magnetron sputtering at a high temperature of 400 ℃ and observed that the growth rate of SiCN film increased with CH_4 flow and decreased with N_2 flow. It has been observed that SiCN thin film deposited using magnetron sputtering possesses higher mechanical properties in the presence of various precursor gases such as C_2H_2, N_2/Ar etc. [8, 26–28]. Park et al. [29] synthesized SiCN film using a laser deposition technique to study the bandgap of the SiCN thin film.

From the literature review, it has been observed that in most of the cases, the synthesis of SiCN thin film has been carried out either using different precursor (in CVD) or various PVD process parameters (target to substrate distance- TSD, bias voltage etc.). However, to the best of the knowledge, the synthesis of SiCN coating in high temperature atmosphere using CVD and its impact on the morphological, structural and mechanical properties of the deposited coating has not been studied by any research group. Therefore, the present experimental work aims the following.

1. To investigate the morphological and structural properties of SiCN thin film coating deposited at different process temperatures (deposition temperature above 850 °C).
2. To investigate the influence of varying deposition temperatures on the compositional and electrochemical properties of SiCN thin film coating.
3. To analyze the results obtained from FTIR and PL spectra analysis and to relate this result with other obtained results.
4. To investigate the different mechanical properties (e.g. hardness, Young's modulus, yield strength, Plasticity index, etc.) of SiCN thin film coating grown with different CVD process temperatures.

NOTE: Before this experimental investigation the synthesis of SiCN thin film was done at a lower temperature range (450°C to 750°C). However, experimental results obtained from various characterization techniques indicate the absence of coating over the substrate and therefore, surface becomes very porous so corrosion resistance was degraded and not found any peaks in PL spectra analysis. The mechanical properties were irregular in nature with regular temperature rise. Then the next set of experiments were carried out at elevated temperatures.

2 Experimental Details

2.1 Preparation of Samples

The deposition of SiCN thin film coating was carried out in a thermal CVD over a p-type c-Si (100) substrate at a varying temperature range and constant N_2 and H_2 gas flow rates. Initially, RCA (Radio Corporation of America) cleaning process was employed to clean the samples.

The coating on the substrate was prepared by using carbon (C) and silicon (Si) (in powder form- very fine powder with size in the range of 25–40 μ) as a base powder in the environment of N_2 and H_2 gas mixture. The powder was mixed in the ratio of 1:1 in a ceramic boat and then the boat was placed behind the substrate. The schematic internal arrangement of the CVD chamber has been shown in Fig. 1.

To remove the residual gases present inside of the CVD chamber, the reactor was pumped out to sub-atmospheric pressure. Within the chamber, base and process pressure were maintained at 3×10^{-6} Torr and 300 mTorr respectively.

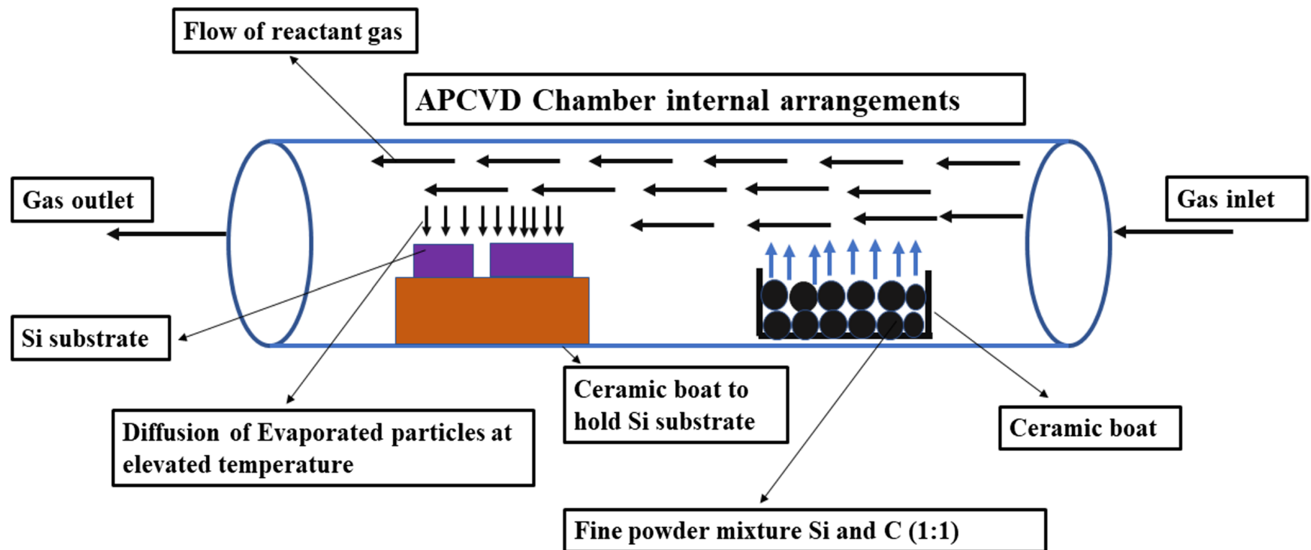

Fig. 1 CVD tube internal view

The flow rate of both carrier gas N_2 (99.99% pure) and precursor gas H_2 (99.99% pure) were maintained at 12 sccm while the deposition temperature was varied from 850 °C to 950 °C. The cooling and heating rate were kept at 5 °C/minute and 3 °C/minute respectively for all the samples.

2.2 Sample Characterization

The morphological analysis of SiCN coating was carried out using Scanning Electron Microscope (SEM) (Model: EVO MA18) attached to Oxford EDS (X-act) with the magnification range of 1 × to 100,000x. In SEM analysis the temperature difference between substrate and source (ΔT) was stimulated at ~ 50 °C. The EDS test was conducted considering 10% instrumental error. In the present work energy of the primary electron is 30 keV.

The thickness of the coating was evaluated by the Dektak profilometer (model Dektak V300) using a diamond stylus having a radius of 2.5 µm. The stylus was kept and moved over the sample at five different locations and the average value considering the values obtained at these locations was taken into consideration.

Particle size and the surface roughness of SiCN coatings were evaluated by Atomic Force Microscopy (AFM) (Model: INNOVA SPM, Brukers) with a scanner of 100 µm. The particle distribution density was measured by using WXFM 5.0 software and it was attached with AFM setup. The scan size area of AFM imaging was 5 μm^2.

The structural property of SiCN was analyzed by X-ray diffraction (XRD) (Model: Bruker D8 Advance X-ray diffractometer) with a wavelength of 0.154 nm. The corresponding diffraction peaks were detected in the 2θ range of 20 to 90 diffraction angle.

The electrochemical corrosion behavior of prepared SiCN samples was measured using CH instrument with the help of CHI software. The experiment was carried out within the range from -0.6 V to -0.4 V vs KCl at room temperature.

The study of the electrochemical behavior of SiCN samples was conducted by using a 1 M H_2SO_4 solution. The solution contained a mixture of distilled water with reagent-grade chemicals. All tests were conducted in a normal atmosphere. Ag/AgCl and platinum wire were worked as reference and counter electrodes respectively while the SiCN samples were used as a working electrode. The scan rate was remained fixed in the range of 0.1 to 0.5 V/s to measure the polarization.

The Fourier Transform Infrared Radiation (FTIR) spectra of SiCN various functional groups were obtained using Perkin Elmer spectrometer instrument (model- Spectrum 2) available with the transmission range of 400 to 4000 cm^{-1} and resolution of 1 cm^{-1}.

A micro-Raman system 1000 of Renishaw was used to measure photoluminescence (PL) spectra at 450 K. As a laser excitation source, the system uses Ar^+ laser with an incident beam of 514.5 nm. It was focused at the time of characterization to a specific region of 1–2 µm in diameter and the spectral resolution was ~ 1.5 cm^{-1}.

The analysis of the mechanical properties of the SiCN coatings was conducted by using the nano-indentation technique (Model: NHTX 55–0019 nano-hardness tester), installed with Berkovich diamond indenter tip (B–I 93; the radius of curvature 20 nm). The maximum load was taken as 85 mN while the loading–unloading rate, load cycle, and

dwell time was fixed as 15 mN/min, 10, and 2 s respectively. The average value of Hardness (H) and Young's modulus (E) were considered for the analysis of other mechanical properties of SiCN coatings.

The measured value of SiCN coating thickness for process temperature has been given below (Table 1):

3 Results and Discussion

3.1 Elemental Composition of SiCN Coating Evaluated using Energy Dispersive Spectroscopy (EDS) technique

The composition of various elements (Si, C, N, and O) of SiCN coating (in atomic %) have been evaluated using EDS technique and is shown in Fig. 2 and Table 2. Test results reveals the atomic % of Si to be maximum followed by N, C and O. EDS results also indicate the presence of less amount of residual oxygen in the coating. In general the beam energy of x-ray (primary electrons) lies within the range of 10 to 30 keV and the size of x-ray generation volume and electron beam interaction volume lies within the range of several µm3 for most of the materials [30]. Now when the penetration depth of primary electrons is more than the particle size there is a chance of fraction of electron beam may get away from the particle before exciting X-rays. This results in the scattering of electron beam out of the particle volume and can be resulted in the excitation of x rays from adjacent particle and substrate [30]. As in the present work the energy of the primary electrons used is 30 keV, hence, the fact of getting higher composition of Si as compared to C, N and O in SiCN thin film is a result of inclusion of Si from the parent substrate which cannot be denied.

Table 1 SiCN Coating thickness

Sample	Temperature (°C)	Flow rate (sccm)	Thickness (µm)
SiCN @ 850 °C	850	12	5.74 ± 0.36
SiCN @ 900 °C	900		5.63 ± 0.29
SiCN @ 950 °C	950		5.28 ± 0.33

Table 2 At. % of Si, C, N, and O in SiCN coating prepared at different temperatures

Sample	Si	N	C	O
SiCN @ 850 °C	66.75	26.26	6.51	0.48
SiCN @ 900 °C	66.37	27.08	5.95	0.60
SiCN @ 950 °C	63.72	27.76	5.49	0.13

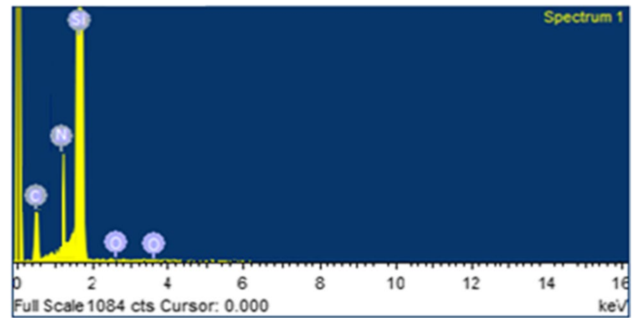

Fig.2 EDS analysis of SiCN coating deposited at 950 °C using CVD

3.2 Surface topography analysis using SEM technique:

The topography of SiCN thin film coating grown at different deposition temperatures is analyzed by scanning electron microscope (SEM) (Fig. 3). The topography of the coating grown at 850 °C is found with the presence of a large number of solid agglomerated particles distributed randomly throughout the coating surface. From the EDS result, it has been confirmed that this agglomeration is the mixture of C and Si particles and the gathering of these agglomerated particles may be due to partial melting and evaporation of the powder particles which may have accumulated as solid agglomeration [31]. The microscopic images of the coating prepared at 900 °C also shows randomly distributed small-sized particles. However, with an increase in process temperature from 900 to 950 °C the gathering of these particles is found to be reduces. The reduction of these agglomerated particles with increasing process temperature may be due to the uniform mixing of C and Si powder at the atomic level. In an earlier published report, it has been reported that the amplitude of vibration of the carbon molecules was found to be increased with rising temperatures which further resulted in a reduction in the mean free path between the layers [32]. SEM images also reveals a pore-free surface. However, with an increase in temperature the size of di-atom (N and C) decreased and hence at 950 °C the di-atomic particles are fine, so the surface of the film is very smooth compared to the films deposited at 850 °C and 900 °C [33]. But still there are some amounts of agglomeration present. This is due to the weak bond or neck exist between the particles with the surface but it has a tendency to become weak with higher temperature [34]. The cross-sectional SEM image of SiCN has been shown in Fig. 3 (b). It demonstrates an example of thin film deposited over the silicon substrate. The system under interrogation consists of SiCN thin film adhere to the surface of the silicon substrate. The layer of coating and substrate is clearly distinguishable due to the presence of significant difference in contrast presented by each

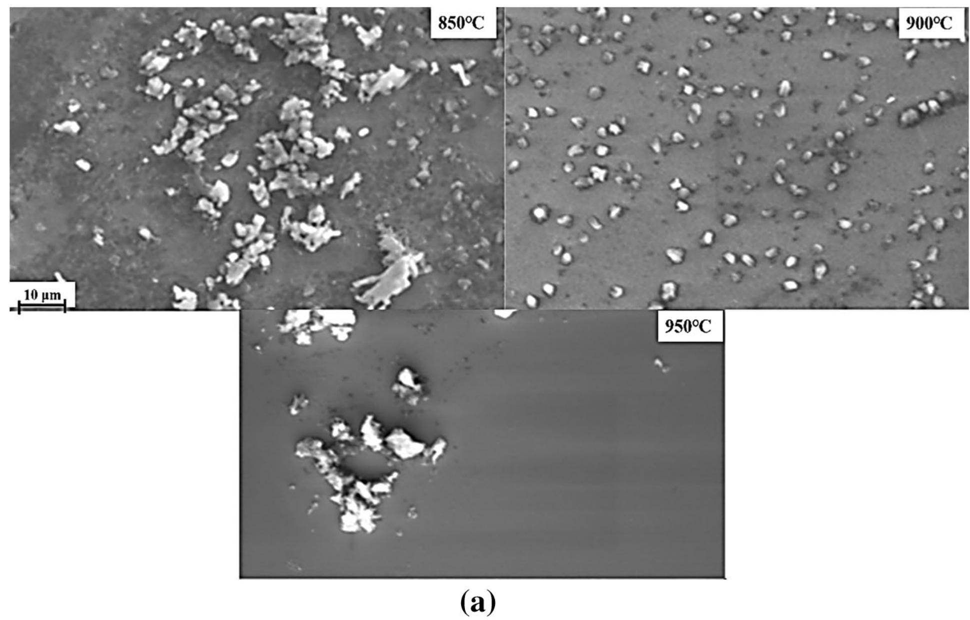

Fig. 3 (**a**) SEM images of SiCN coating deposited under different temperature. (**b**) Cross-sectional SEM image of SiCN coating

material. It is clear from cross sectional surfaces of this film that the formed surface is irregular in nature. Irregularity in the surface pattern has been reduced with higher temperature but the formation of dense microstructure particularly at coating-substrate interface is visible from Fig. 3 (b). It has been observed that higher temperature helps to reduce the coating thickness (Table 1) and this is also evident from cross sectional figures. This is due to under high temperature material quality is enhanced in terms of micro and macro structural features e.g. porosity, density, intra and inter granular pore distribution, phases, etc. to produce homogeneous and compact materials. Moreover, due to higher temperature

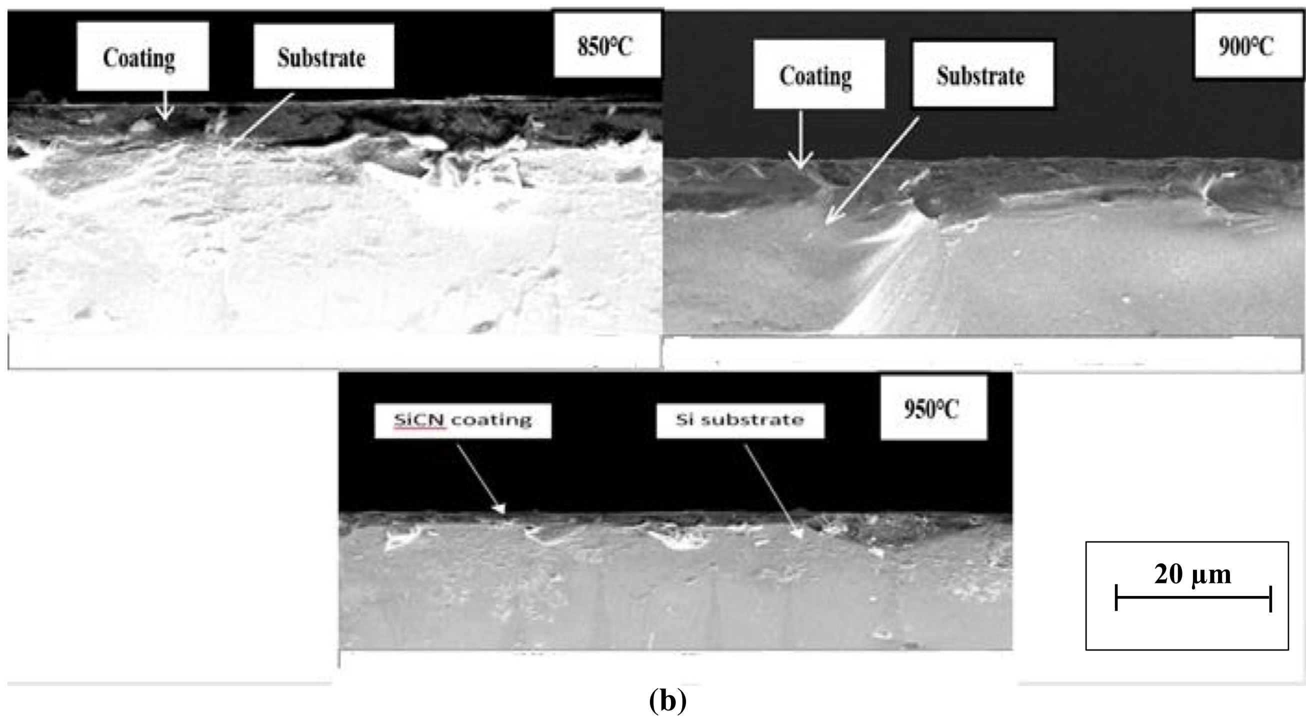

Fig. 3 (continued)

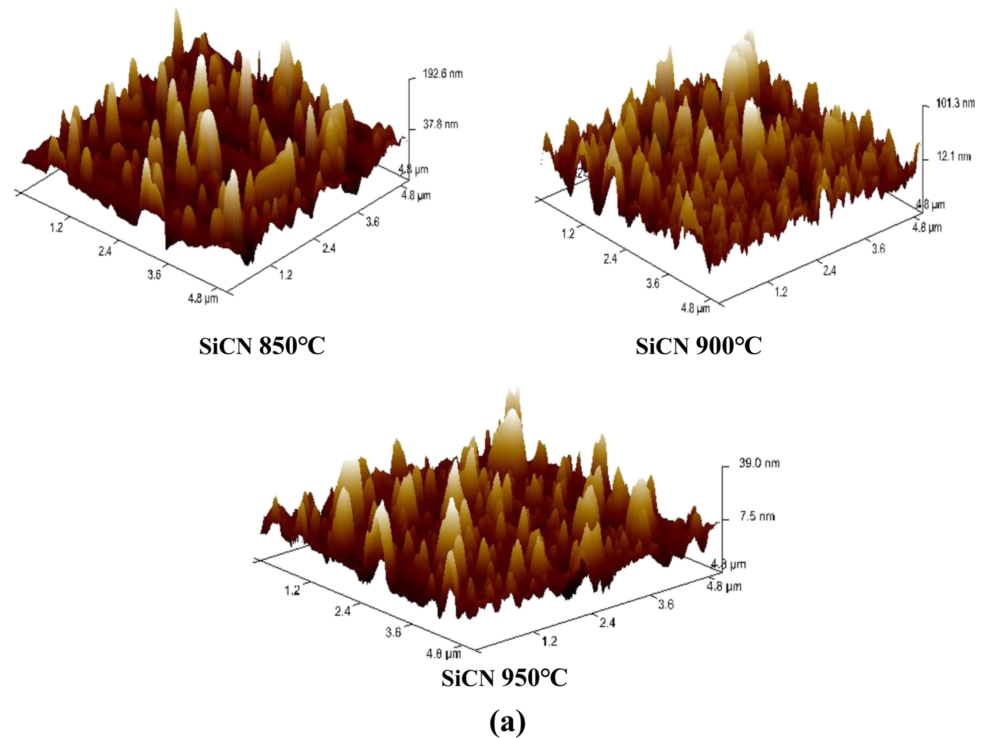

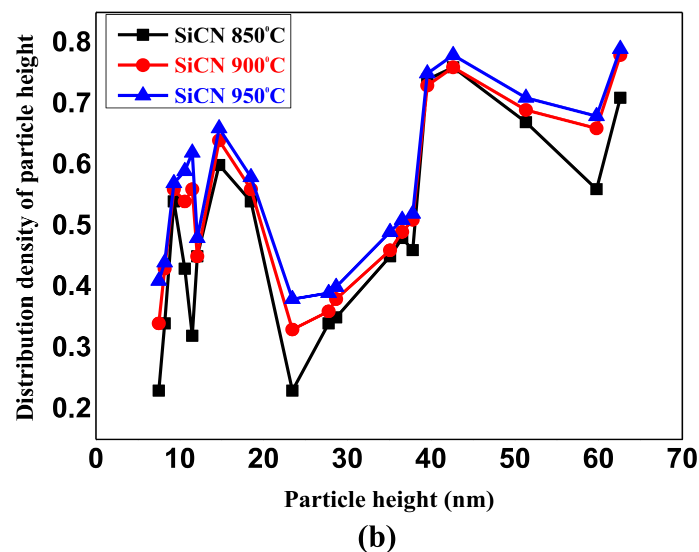

Fig. 4 (**a**) AFM images of SiCN coating deposited under different temperature. (**b**) Particle distribution density obtained from AFM

materials have been transformed into more ordered phase, so the defects reduce and dimensional changes take place due to shrinkage. Due to the shrinkage thickness ultimately decreases.

3.3 Morphology analysis using AFM technique

The estimation of particle height of SiCN coating with varying process temperature was carried out using AFM and is shown in Fig. 4. The results indicate that the shape of the particles of entire deposited SiCN comprised of conical or pyramidal-shaped grains of different sizes. With the increase in process temperature, it has been observed that the particle height of the SiCN coating is decreasing. The maximum and the average particle height of the SiCN coating deposited at 850 °C, 900 °C and 950 °C are found as 62.6 and 37.8 nm, 51.3 and 12.1 nm, 39 and 7.5 nm respectively. The particle distribution density is highlighted in Fig. 4(b) where X-axis represents the particle height and Y-axis represents

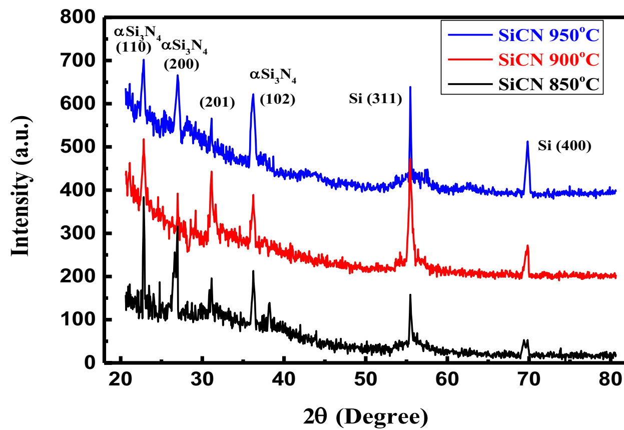

Fig. 5 XRD pattern of SiCN coating deposited under different temperature

the corresponding density. It has been observed that the particle distribution density increases with the process temperature i.e., the particle distribution density of SiCN coating at 850 °C is less compared to that grown at 900 °C which is again less compared to that grown at 950 °C. The variation in distribution density with increasing process temperature may be due to the increase in the randomness of the gaseous molecules (as the volume of the CVD chamber remained the same), which may have increased the frequency of the collision among the gaseous molecules. The higher penetration over the parent substrate may have been caused due to the frequent collision among the Si, C, and N molecules which may be the reason behind the dense gathering of particles with the consecutive reduction in size. The surface roughness (R_a) value which is the arithmetic mean deviation of surface profile was observed to be reduced from 21.6 to14.2 nm with an increase in process temperature from 850 to 950 °C.

3.4 Microstructural property analysis of SiCN coating by X-ray diffraction (XRD) technique

The X-ray diffraction (XRD) patterns are recorded to analyze the microstructural properties of SiCN coating at different temperatures is shown in Fig. 5. The diffraction peaks of the SiCN coating grown at 850℃, 900℃ and 950℃ are observed at 22.82, 26.97, 31.13, 36.23, 55.46 and 69.2 corresponding to (110), (200), (201), (102), (311) and (400) crystal planes respectively [35, 36]. The SiCN diffraction pattern at 22.82, 26.97 and 36.23 is attributed to the α-Si_3N_4 phase. The diffraction pattern of SiCN film prepared at the process temperature of 850 °C at (110) diffraction plane shows higher peak intensity as compared to thin-film grown at 900 °C and 950 °C for the same diffraction phase, indicating higher crystallinity of the coating [37]. It has been noticed that full width at half maxima (FWHM) of the diffraction peaks in the range of 21—22, 30-31, 35-37 and 68-69 increases from 0.33–1.26, 0.47–1.14, 0.56–1.32 and 0.79–1.26 respectively with an increase in process temperature from 850 to 950℃. The broadening of the diffraction peak with an increase in process temperature indicates the reduction of crystallite size and it is in good agreement with the calculated results shown in Table 3. Peak broadening in XRD is also an indication of crystal structure refinement and elevated plastic deformation of the thin film due to consecutive intensification in the dislocation density [38]. The crystallite size of the coating has been evaluated using Scherrer's equation and is given by

$$D = \frac{0.9 * \lambda}{\beta'_{hkl} \times cos\theta} \quad (1)$$

D: Crystallite size, λ: wavelength of Cu-Kα radiation = 1.54 Å, β_{hkl}: FWHM of the diffraction peak.

Here β_{hkl} has been evaluated using the relation

$$\left(\beta_{hkl}\right)^2 = \left(\beta_{instrumental}\right)^2 - \left(\beta_{experimental}\right)^2 \quad (2)$$

$\beta_{instrumental}$ is the instrumental broadening factor.

From Scherrer's model, it has been observed that with an increase in process temperature the average crystallite size of SiCN coated thin films gradually decreases. The crystallite size reduction with higher temperature is associated with phenomena of the mean free path of the molecules and Knudsen law (Cosine law) as presented by the equation:

Table 3 Crystallite size of SiCN thin film grown at varying Temperature (nm)

Temperature	SiCN (110)	SiCN (200)	SiCN (201)	SiCN (102)	SiCN (400)
850 °C	24.51	18.52	17.50	14.90	12.18
900 °C	7.42	7.45	6.75	8.73	8.08
950 °C	6.42	5.19	7.22	6.32	7.66

Table 4 Inter planner spacing of SiCN coating grown at varying Temperature (nm)

Temperature	SiCN (110)	SiCN (200)	SiCN (201)	SiCN (102)	SiCN (400)
850 °C	0.4	0.33	0.29	0.25	0.13
900 °C	0.4	0.33	0.29	0.24	0.13
950 °C	0.4	0.34	0.29	0.25	0.13

Table 5 The lattice parameter of SiCN coating grown at varying Temperature (nm)

Temperature	SiCN (110)	SiCN (200)	SiCN (201)	SiCN (102)	SiCN (400)
850 °C	0.56	0.67	0.65	0.56	0.60
900 °C	0.56	0.66	0.65	0.53	0.57
950 °C	0.57	0.68	1.46	0.56	0.57

Table 6 Comparison in the crystallite size of SiCN coating using the Scherrer's and UDM model

Sl. No	Coating	Deposition Temperature (°C)	Crystallite size (D) in nm	
			Scherrer method	UDM model
1	SiCN	850	17.52	20.533
2		900	8.32	9.05
3		950	6.56	7.33

$$\lambda' = k_B T / \sqrt{2}\left(\pi P D^2\right) \tag{3}$$

λ': mean free path, D: molecular diameter, T: temperature., P: pressure, k_B: Boltzmann constant.

As the process temperature increases from 850 to 950 °C the C and Si molecules attained higher thermal energy in their evaporated state which results in higher intensity molecular collision and thus increases the mean free path. Also, the rise in process temperature results in a consecutive increase in molecular mean velocity (U_v) as well as the force of impingement over the substrate for a unit area.

The interplanner distance and lattice constant of SiCN coating have been represented in Table 4 and Table 5. Here it has been found that the higher process temperature has lower influence on these parameters.

3.4.1 Estimation of crystallite size using the Williamson hall (W–H) method

W–H model is a theoretical method used to evaluate the crystallite size and the associated elastic properties of the coating. Here a comparative analysis has been made in

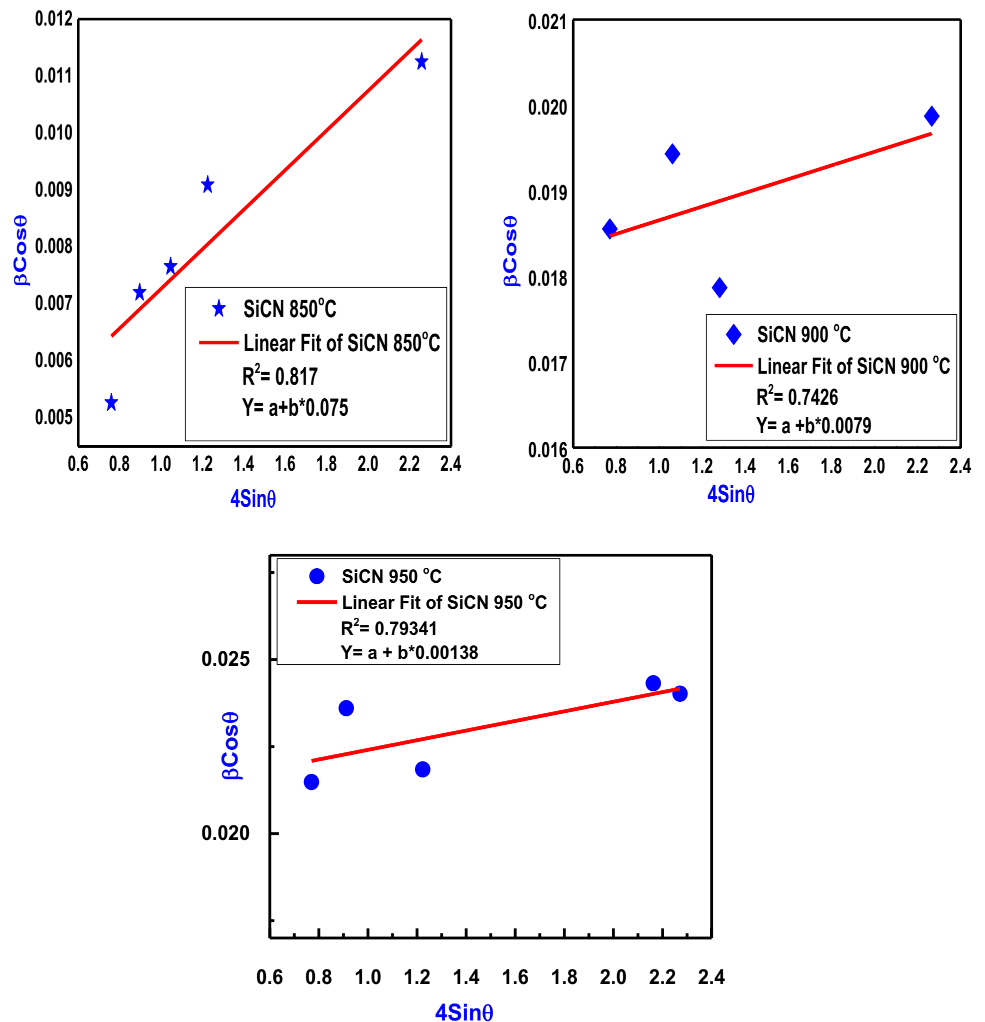

Fig. 6 UDM plot of SiCN XRD peak deposited at different temperature

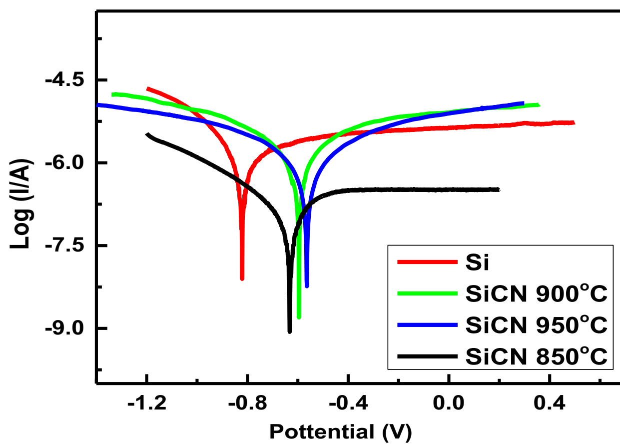

Fig. 7 Taffel plot of SiCN coatings deposited under different temperature

between experimental results with the theoretical results based upon the W–H method. This method is comprised of three models those are: uniform deformation model (UDM), uniform stress deformation model (USDM) and uniform deformation energy density model (UDEDM) [39]. Here in this work, only the UDM model is used to estimate the crystallite size of the coating. The UDM model was developed with an assumption that the strain induced in the crystals was equal in all directions and peak broadening in XRD was due to the presence of the induced strain along with the crystallographic directions and is given by:

$$\beta_{hkl}\cos\theta = \frac{k\lambda}{D} + 4\epsilon \times \sin\theta \tag{4}$$

where ε: strain induced in the coating.

Based on Eq. 4 a plot between β_{hkl} $cos\theta$ (y-axis) and $4\varepsilon \times \sin\theta$ (x-axis) is obtained where the slope of the straight line indicates the intrinsic strain induced in the coating. The correlational coefficient R^2 and slope of the fitted line are shown in Fig. 6. The presence of intrinsic/lattice strain may be due

Fig. 8 Deconvoluted FTIR plot of SiCN thin film coating deposited at different temperature

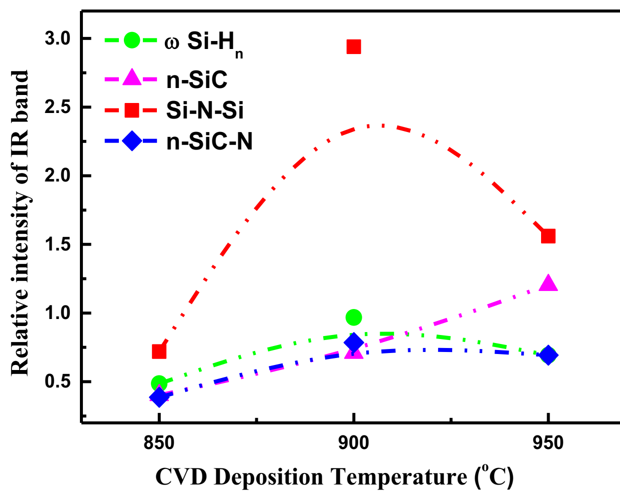

Fig. 9 Peak intensity of deconvoluted FTIR spectrum of SiCN coating to process temperature

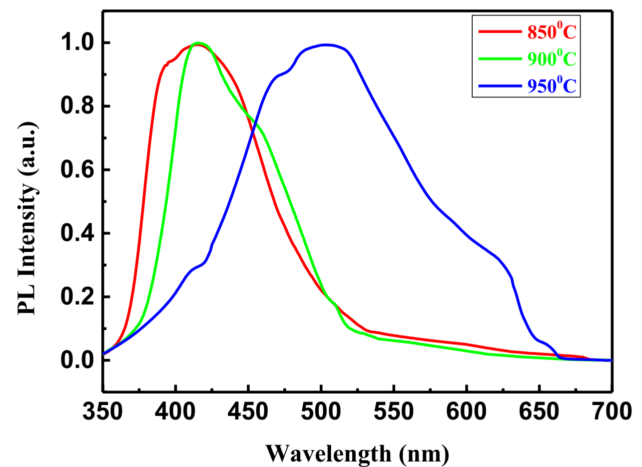

Fig. 10 PL spectra of SiCN thin film deposited at different temperature

to lattice expansion and contraction due to size confinement. Past research work reported that the size confinement may be take place due to slight modifications in the crystal arrangements [40]. The presence of lattice strain due to size confinement may also be take place due to various crystal defects [40]. From Fig. 5 it is observed that the slope of the fitted line for all the coatings are positive, therefore it indicates lattice expansion [41]. The positive slope obtained for the fitted line in each case also indicates the presence of tensile stress in the coating [42]. Here the slope of the fitted line of SiCN coating grown at 850 °C, 900 °C and 950 °C are observed as 0.075, 0.0079 and 0.00138 respectively. With an increase in process temperature the crystallite size evaluated using the UDM model and from Scherrer's equation is shown in Table 6.

3.5 Electrochemical corrosion analysis of SiCN coating deposited at different process temperatures

In Fig. 7, the potentiodynamic polarization curves indicates the electrochemical properties of pure Si, SiCN at 850 °C, 900 °C and 950 °C. Originally the corrosion potential for Si at normal temperature is found almost near to -0.83 V. After the deposition of SiCN film at the higher temperature, the corrosion potential is shifted towards -0.51 V with relatively low corrosion activities. It depicted that with an increase in temperature it is able to improve the anticorrosion property under appropriate growth conditions [42]. The increase in temperature ultimately enhanced the reaction rate by a factor of ten which improved the activation energy between the molecules and thus enhanced the anticorrosion property [43]. This improved corrosion protection is due to the increase in the thickness of the deposited coating which is made possible with higher temperature [44].

3.6 Analysis of Fourier Transform Infrared Radiation (FTIR)

The FTIR spectra of CVD deposited SiCN coating deposited at varying process temperatures has been shown in Fig. 8. Overall, there are three major vibrational signatures observed within the range of 600 cm^{-1} to 1100 cm^{-1}. The vibrational signature observed in the coatings prepared at varying process temperatures in the range of 600 cm^{-1} to 700 cm^{-1} is attributed to Si-H_n wagging vibration [45]. The peak signature observed within the range of 780 cm^{-1} to 1100 cm^{-1} corresponding to Si–C stretching and SiC-N stretching respectively [46]**.** For the further analysis of bond vibration in the coating, the broad vibrational signatures have been deconvoluted into four Lorentzian peaks within the range of 600 cm^{-1} to 1100 cm^{-1}. The peak observed within 700 cm^{-1} to 730 cm^{-1} (green peak in all the coatings) is attributed to Si–H rocking and wagging vibration [47].

The absorption spectra centered within 740 cm^{-1} to 781 cm^{-1} can be attributed to Si–C stretching and wagging vibrations [47]. Peak signature centered within 866.37 cm^{-1} can be attributed to SiC-N stretching vibration [47, 48]. The introduction of nitrogen atoms with an increase in deposition temperature in the CVD chamber during deposition resulted in upshifting and broadening of Si–C bonds due to the formation of Si–N bonds. Figure 3, a graph has been plotted in between a relative peak intensity of the deconvoluted peak signature of various bonds of SiCN coating to process temperature. From Fig. 9 it has been observed that with an increase in process temperature the intensity of Si–C band found to be increased and reached its maximum value for

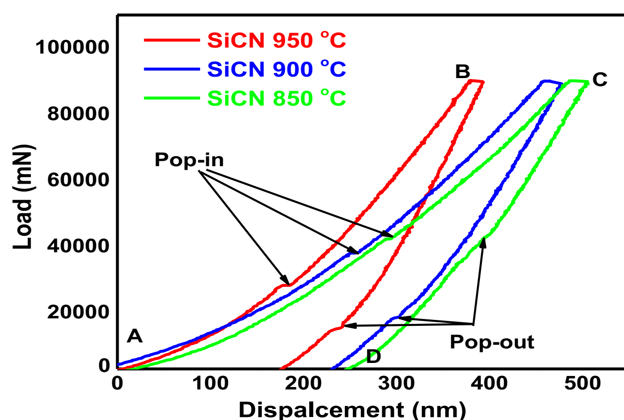

Fig. 11 Loading–Unloading plot of SiCN coating

coating synthesized at 950 °C. However, the peak intensity of other deconvoluted bands (Si–H Si–N-Si and SiC-N) with increasing process temperature are initially observed to be increased till 900 °C and then reduced with further increase in process temperature. The deconvoluted band signature obtained for different coatings synthesized at different process temperatures also indicates that the peak intensity of the Si–N-Si functional group is comparatively higher than the intensity of the rest of the functional groups (Si–H Si–C and SiC-N). The higher intensity of the Si–N-Si group indicates a higher amount of nitrogen in the coating and is directly related to the properties of the film. This result is also in good agreement with the EDS result as shown in Fig. 2 in Sect. 3.1. The decrease in the intensity of functional groups (Si–H, Si–N-Si and SiC-N) above 850 °C may be due to higher temperature-induced crosslinking reactions which may have resulted in the growth of Si–C bond with increased intensity.

3.7 Analysis of photoluminescence spectroscopy of SiCN thin film coating

The photoluminescence (PL) spectroscopy of SiCN thin film coating deposited under different substrate temperatures is shown in Fig. 10. The complex structure of the materials is responsible for the presence of different single, asymmetric and broad band and these can be identified by PL spectra. These are usually comprising of different overlapped component emission signals those are developed due to the presence of various delocalized states of SiCN coating. The intensity of peak position of PL spectra for all the SiCN coatings deposited under different temperatures are found to be almost same and it is ~ 1. The peak position of PL spectra for 850 °C and 900 °C are observed at 415 and 418 nm respectively whereas the peak position for 950 °C is observed at 504 nm. So, it has been observed that with higher deposition temperature PL spectra has been blue-shifted towards higher wavenumber. A similar type of results was observed by Wrobel et al. [49] in their work. This blue shift in PL spectra may be defined as a function of laser power. The blue shift in PL spectra with higher laser power indicates the occurrence of radiative recombination due to the presence of defects in donor/acceptor pair level. The reason behind of defects at the donor/acceptor level is due to the interaction of coulomb in between. Higher laser power generally increased the number of excited carriers hence the distance in between them is decreases. Now if radiative recombination is takes place in between donor/acceptor pair level defects then time-dependent PL peaks will give some additional evidence in a form of a blue shift.

3.8 Analysis of Mechanical property of SiCN coating by Nanoindentation technique

The analysis of different mechanical properties of SiCN coating grown at different process temperatures were done by the nano-indentation analysis and the graph between the indentation load (P) and indentation depth (h) has been shown in Fig. 11. The coatings prepared at 850 °C, 900 °C and 950 °C are subjected to maximum penetration depth (h_{max}) of 490.6, 468.9 and 379.1 nm respectively. The decrease in penetration depth with an increase in process temperature indicates an increase in coating hardness with increasing process temperature. The indenter was allowed to penetrate over the coating thickness up to 9% of the overall coating thickness to avoid the effect of substrate properties on the results.

The area under the indentation curve ABCD is shown in Fig. 11 represented the overall plastic deformation where the curve AB indicates elastoplastic loading and the curve CD represents elastoplastic unloading. As the indentation load reached the maximum value (P_{max}) the indenter was held for a few seconds to avoid continuous sinking of the indenter towards the coating's surface because of time-dependent deformation [50]. The flat section from B to C usually represents the creep behavior of the material but as SiCN is hard coating materials it is eventually the result of thermal drift [42]. During loading and unloading of the indenter, pop-in and pop-out phenomena are observed for all the coatings deposited under different process temperatures. The pop-in behavior in SiCN coating prepared at 850 °C, 900 °C and 950 °C are observed at 290.05, 251.28 and 179.8 nm respectively. In past research work, it has been reported that this pop-in behavior indicates the start of plastic deformation in the coating. As the indenter load reached a critical value, the ultimate shear stress at the atomic level surpassed the theoretical shear strength which resulted in consecutive homogenous dislocation and nucleation throughout the crystals [51]. During the

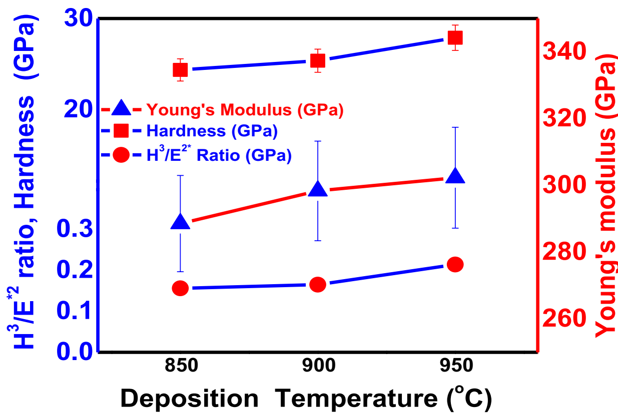

Fig. 12 Change of Hardness, Young's modulus and plastic deformation index with temperature

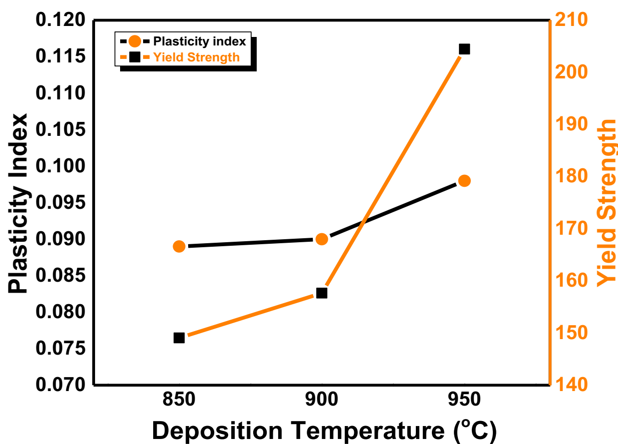

Fig. 13 Change of yield strength and plasticity index under different temperature

unloading of the indenter, another phenomena known as pop out is observed in all the coatings which may be due to phase transformation of SiCN i.e. Si-II to Si-III and Si-XII [52]. Hu et al. [53] reported that the phase transformation of Si in diamond anvil cells from Si-II to less dense phase of Si-III and Si-XII.

The H and E of the deposited coating are evaluated by using the theory given by Oliver and Pharr method [54]. The experimental value of H and E are calculated using the following equations:

$$H = \frac{P_{max}}{A} \tag{5}$$

$$S = \frac{dp}{dh} = 2\beta\sqrt{\frac{A}{\pi}}E_r \tag{6}$$

$$\frac{1}{E_r} = \frac{1 - v_f^2}{E_f} + \frac{1 - v_{id}^2}{E_{id}} \tag{7}$$

Here, P_{max} : maximum indentation load over the coating, A: contact area of indenter with the sample surface, S: measured contact thickness from load and displacement plot, β: indenter constant and is equal to 1.034 for Berkovich indenter, E_r: reduced elastic modulus and the corresponding f and id represents the film and indenter respectively [55]. During the calculation of H and E_f value of SiCN thin-film coating, the Poisson's ratio and Young's modulus of Berkovich indenter are considered as 0.07 and 1141 GPa respectively. The measured values of hardness for SiCN thin-film coating are 24.36, 25.57 and 27.89 GPa for the film deposited at the temperature of 850 °C, 900 °C, and 950 °C respectively. The Young's modulus of SiCN coating deposited at 850 °C, 900 °C and 950 °C are 288.56, 298.35 and 302.30 GPa respectively. The variation of H and E_f with different deposition temperatures is shown in Fig. 12. It has been observed that the value of hardness and Young's modulus are increases with higher deposition temperature this may be due to the formation of the dense microstructure of the film under higher deposition temperature.

The plastic deformation resistance ($\frac{H^3}{E^{*2}}$) act as an index against the plastic deformation of the material. Here (E^*) indicates the effective modulus of the film and evaluated by using the following Eq.:

$$E^* = \frac{E_f}{1 - \upsilon^2} \tag{8}$$

where υ poison's ratio of the film and is equal to 0.205 [55]. The variation of the plastic deformation index with different deposition temperatures is shown in Fig. 11.

The Yield strength of the materials is related to the plastic deformation index by the following relationship [50]

$$\sigma_y = 0.78a^2\left(\frac{H^3}{E^{*2}}\right) \tag{9}$$

Here, 'a' represents the indenter radius at contact depth (h_c) and the value of 'a' is varying within the range of 20 to 50 nm. The Yield strength value of SiCN thin film deposited at 850℃, 900℃ and 950℃ are 149.058, 157.65 and 204.47 GPa respectively (Fig. 13).

The ratio of hardness (H) to reduced modulus (E_r) is a very important parameter to judge the behavior of the materials against wear. The H/E_r ratio is known as the plasticity index of the materials. Where E_r is measured as [50]

$$E_r = \frac{S\sqrt{\pi}}{2\sqrt{A_C}} \tag{10}$$

The variation in plasticity index with deposition temperature has been shown in Fig. 13.

The plastic deformation is the reason behind of gradual material removal or gradual wear but elastic deformation is not responsible for this. The film which possesses the highest H/E_r ratio would be having more elastic deformation [50]. Here it is applicable for the SiCN thin film deposited at 950 °C. Whereas the small value of H/E_r, comes under the large fraction of work then the degree of deformation is also the same [56]. The ratio in between h_f/h_{max} is a paramount parameter to judge the unrecoverable strain which is linked with the H/E_r ratio by the following Eq. (11) [50]

$$\frac{h_f}{h_{max}} \infty \frac{W_t - W_r}{W_t} \infty \frac{H}{E_r} \tag{11}$$

So, the maximum plastic strain was expectable from a smaller H/E_r ratio. Therefore, it's very much obvious that the materials which possess a higher H/E_r ratio must have less accumulative strain and strain energy which ultimately helped to provide higher wear resistance property [50, 56]. So, the SiCN film which was deposited at 950℃ must be possessed higher wear resistance as it has maximum plasticity index.

4 Conclusion

SiCN thin film coating was deposited on Si substrate by CVD process under different deposition temperatures. The compositional analysis by the EDS technique confirms the maximum content present in SiCN is Si followed by N, C and this result is very much justified by the FTIR analysis. The SEM images confirm reduced number of agglomerated particles with higher deposition temperatures. AFM analysis confirms the enhancement of particle distribution density with higher deposition temperature. Structural analysis through XRD reveals the enhancement of FWHM of different diffraction planes with higher deposition temperatures. The PL spectra analysis confirms the blue shift of PL peaks with higher temperatures. The IR spectra reveals the higher intensity of the Si–N functional group compared to Si–C and Si–H. Mechanical property analysis confirms the superiority of SiCN thin film coating deposited at 950 °C over other SiCN thin film coatings.

Acknowledgements NA

Authors' contributions **Soham Das:** Conceptualization, Methodology, Software, Writing, **Dhruva Kumar:** Writing, Methodology, Reviewing, Supervision **Rishikesh Borah:** Writing, Data Curation, Methodology, **Abhinov Dutta:** Writing, Data Curation, Methodology, **Spandan Guha:** Writing, Visualization, Investigation, Editing.

Funding No Funding has been received for this work.

Availability of data and materials NA.

Declarations

Ethics approval NA

Consent to participate NA

Consent for publication In accordance with copyright transfer rules.

Conflict of Interest The authors declare that they have no conflict of interest.

References

1. Feng Y, Guo X, Gong H, Zhang Y, Liu Y, Lin X, Mao J (2018) The influence of carbon materials on the absorption performance of polymer-derived SiCN ceramics in X-band. Ceram Int. https://doi.org/10.1016/j.ceramint.2018.05.240
2. Xue J, Yin X, Cheng L (2019) Induced crystallization behavior and EMW absorption properties of CVI SiCN ceramics modified with carbon nanowires. Chem Eng J. https://doi.org/10.1016/j.cej.2019.122213
3. Ctvrtlik R, Al-Haik MS, Kulikovsky V (2015) Mechanical properties of amorphous silicon carbonitride thin films at elevated temperatures. J Mater Sci. https://doi.org/10.1007/s10853-014-8715-0
4. Badzian A, Badzian T, Drawl WD, Roy R (1998) Silicon carbonitride: a rival to cubic boron nitride. Diam Relat Mater. https://doi.org/10.1016/S0925-9635(98)00228-3
5. An L, Riedel R, Konetschny C, Kleebe HJ, Raj R (1998) Newtonian viscosity of amorphous silicon carbonitride at high temperature. J Am Ceram Soc. https://doi.org/10.1111/j.1151-2916.1998.tb02489.x
6. Riedel R, Kleebe HJ, Schönfelder H, Aldinger F (1995) A covalent micro/nano-composite resistant to high-temperature oxidation. Nature. https://doi.org/10.1038/374526a0
7. Bielinski, D., Wrobel, A. M., Walkiewicz-Pietrzykowska, A.: Mechanical and tribological properties of thin remote microwave plasma CVD a-Si: N: C films from a single-source precursor. Tribol. Lett. (2002) 71–76. https://doi.org/10.1023/A:1020144313969
8. Hoche H, Allebrandt D, Bruns M, Riedel R, Fasel C (2008) Relationship of chemical and structural properties with the tribological behavior of sputtered SiCN films. Surf Coat Technol. https://doi.org/10.1016/j.surfcoat.2008.06.126
9. Tomasella E, Spinelle L, Bousquet A, Rebib F, Dubois M, Eypert C, Sauvage T (2009) Structural and optical investigations of silicon carbon nitride thin films deposited by magnetron sputtering. Plasma Processes Polym. https://doi.org/10.1002/ppap.200930103
10. Liew LA, Liu Y, Luo R, Cross T, An L, Bright VM, Raj R (2002) Fabrication of SiCN MEMS by photopolymerization of pre-ceramic polymer. Sens Actuators A. https://doi.org/10.1016/S0924-4247(01)00723-3
11. Carreño MNP, Lopes AT (2004) Self-sustained bridges of a-SiC: H films obtained by PECVD at low temperatures for MEMS applications. J Non-Cryst Solids. https://doi.org/10.1016/j.jnoncrysol.2004.03.026
12. Mehregany M, Zorman CA (1999) SiC MEMS: opportunities and challenges for applications in harsh environments. Thin Solid Films. https://doi.org/10.1016/S0257-8972(99)00374-6
13. Soltani N, Bahrami A, Pech-Canul MI, González LA, Gurlo A (2017) Kinetics of Silicon Nitride Formation on SiO_2-Derived

Rice Husk Ash Using the Chemical Vapor Infiltration Method. Int J Chem Kinet. https://doi.org/10.1002/kin.21075
14. Leo A, Andronenko SI, Stiharu R, Bhat B (2010) Characterization of thick and thin film SiCN for pressure sensing at high temperatures. Sensors. https://doi.org/10.3390/s100201338
15. Yang J (2013) A harsh environment wireless pressure sensing solution utilizing high temperature electronics. Sensors. https://doi.org/10.3390/s130302719
16. Soltani N, Bahrami A, Pech-Canul MI, González LA, Gurlo A (2018) Surface modification of rice-husk ash (RHA) by Si_3N_4 coating to promote its wetting by Al-Mg-Si alloys. Mater Chem Phys. https://doi.org/10.1016/j.matchemphys.2017.10.009
17. Soltani N, Bahrami A, Pech-Canul MI, Gonzalez LA (2020) Improving the Interfacial Reaction between Cristobalite Silica from Rice Husk and Al–Mg–Si by CVD-Si_3N_4 Deposition. Waste Biomass Valor. https://doi.org/10.1007/s12649-019-00706-w
18. Peng X, Song L, Le J, Hu X (2002) Spectra characterization of silicon carbonitride thin films by reactive radio frequency sputtering. J Vac Sci Technol B. https://doi.org/10.1116/1.1431952
19. Wrobel AM, Błaszczyk-Łe I, Walkiewicz-Pietrzykowska A, Bieliński DM, Aoki T, Hatanaka Y (2004) Silicon carbonitride films by remote hydrogen-nitrogen plasma CVD from a tetramethyldisilazane source. J Electrochem Soc. https://doi.org/10.1149/1.1805522
20. Awad Y, El Khakani MA, Aktik C, Mouine J, Camiré N, Lessard M, Smirani R (2009) Structural and mechanical properties of amorphous silicon carbonitride films prepared by vapor-transport chemical vapor deposition. Surf Coat Technol. https://doi.org/10.1016/j.surfcoat.2009.08.032
21. Badzian A, Badzian T, Roy R, Drawl W (1999) Silicon carbonitride a new hard material and its relation to the confusion about harder than diamond C_3N_4. Thin Solid Films. https://doi.org/10.1016/S0040-6090(99)00535-0
22. Kumar D, Ghadai RK, Das S, Sharma A, Swain BP (2019) Effect of nitrogen flow rate on the mechanical properties of CVD-deposited SiCN thin films. Bull Mater Sci. https://doi.org/10.1007/s12034-019-1937-7
23. Swain BP, Hwang NM (2008) Study of structural and electronic environments of hydrogenated amorphous silicon carbonitride (a-SiCN: H) films deposited by hot wire chemical vapor deposition. Appl Surf Sci. https://doi.org/10.1016/j.apsusc.2008.02.077
24. Zhao W, Shan X, Zhang Z, Zhai C, Yun J, Qu Y (2014) Structural and chemical analysis of ternary SiC_XN_Y thin films deposited by improved hot filament chemical vapour deposition. Mater Res Innovations. https://doi.org/10.1179/1432891714Z.000000000836
25. Bachar A, Bousquet A, Mehdi H, Monier G, Robert-Goumet C, Thomas L, Tomasella E (2018) Composition and optical properties tunability of hydrogenated silicon carbonitride thin films deposited by reactive magnetron sputtering. Appl Surf Sci. https://doi.org/10.1016/j.apsusc.2018.03.040
26. Hänninen T, Schmidt S, Ivanov IG, Jensen J, Hultman L, Högberg H (2018) Silicon carbonitride thin films deposited by reactive high power impulse magnetron sputtering. Surf Coat Technol. https://doi.org/10.1016/j.surfcoat.2017.12.037
27. Sundaram KB, Alizadeh Z, Todi RM, Desai VH (2004) Investigations on hardness of rf sputter deposited SiCN thin films. Mater Sci Eng A. https://doi.org/10.1016/j.msea.2003.09.103
28. Ma Z, Zhou J, Chen Z, Xie E (2011) Luminescence properties of terbium-doped SiCN thin films by rf magnetron reactive sputtering. Diam Relat Mater. https://doi.org/10.1016/j.diamond.2011.01.041
29. Park NM, Kim SH, Sung GY (2003) Band gap engineering of SiCN film grown by pulsed laser deposition. J Appl Physics. https://doi.org/10.1063/1.1594267
30. Valdrè, G., Moro, D., Ulian, G.: Monte Carlo simulation of the effect of shape and thickness on SEM-EDS microanalysis of asbestos fibres and bundles: the case of anthophyllite, tremolite and actinolite. IOP Conf. Ser.: Mater. Sci. Eng. (2018). https://doi.org/10.1088/1757-899X/304/1/012019
31. Das S, Guha S, Ghadai R, Kumar D, Swain BP (2017) Structural and mechanical properties of CVD deposited titanium aluminium nitride (TiAlN) thin films. Appl Phys A. https://doi.org/10.1007/s00339-017-1032-0
32. Kellett EA, Jackets BP, Richards BP (1964) A study of the amplitude of vibration of carbon atoms in the graphite structure. Carbon. https://doi.org/10.1016/0008-6223(64)90058-2
33. Montagnes DJ, Franklin M (2001) Effect of temperature on diatom volume, growth rate, and carbon and nitrogen content: reconsidering some paradigms. Limnol Oceanogr. https://doi.org/10.4319/lo.2001.46.8.2008
34. Viera G, Bertran E, Polo M, Garcia-Caurel E, Farjas J, Roura P (2000) Thermal Stabilization and Crystallization of Nanometric Particles of Si-C-N Produced by RF-Plasma Enhanced Chemical-Vapor-Deposition. MRS Proc. https://doi.org/10.1557/PROC-609-A24.5
35. Fainer NI, Rumyantsev YM, Golubenko AN, Kosinova ML, Kuznetsov FA (2003) Synthesis of nanocrystalline silicon carbonitride films by remote plasma enhanced chemical vapor deposition using the mixture of hexamethyldisilazane with helium and ammonia. J Cryst Growth. https://doi.org/10.1016/S0022-0248(02)02041-9
36. Fainer NI, Kosyakov VI, Rumyantsev YM, Maximovskii EA, Prokhorova SA, Gevko PN (2012) Composition and structure of silicon carbonitride layers grown on Si (100)/(Fe, N, Co) substrates. J Struct Chem. https://doi.org/10.1134/S0022476612040282
37. Das, S., Guha, S., Das, P. P., Ghadai, R. K.: Analysis of morphological, microstructural, electrochemical and nano mechanical characteristics of TiCN coatings prepared under N_2 gas flow rate by chemical vapour deposition (CVD) process at higher temperature. Ceram. Int. (2020) 10292. https://doi.org/10.1016/j.ceramint.2020.01.023
38. Vashista M, Paul S (2012) Correlation between full width at half maximum (FWHM) of XRD peak with residual stress on ground surfaces. Philos Mag. https://doi.org/10.1080/14786435.2012.704429
39. Das S, Guha S, Ghadai R, Sharma A, Chatterjee S (2020) Morphological mechanical property analysis and comparative study over structural properties of CVD TiN film grown under different substrate temperature in nitrogen gas atmosphere. SILICON. https://doi.org/10.1007/s12633-020-00807-5
40. Nath D, Singh F, Das R (2020) X-ray diffraction analysis by Williamson-Hall Halder-Wagner and size-strain plot methods of CdSe nanoparticles-a comparative study. Mater Chem Phys. https://doi.org/10.1016/j.matchemphys.2019.122021

41. Sarkar S, Das R (2018) Shape effect on the elastic properties of Ag nanocrystals. Micro Nano Lett. https://doi.org/10.1049/mnl.2017.0349
42. Guha S, Das S, Bandyopadhyay A, Das S, Swain BP (2018) Investigation of structural network and mechanical properties of Titanium silicon nitride (TiSiN) thin films. J Alloy Compd. https://doi.org/10.1016/j.jallcom.2017.09.340
43. Huang WH, Lin CH, Lin BS, Sun CL (2018) Low-temperature CVD graphene nanostructures on Cu and their corrosion properties. Materials. https://doi.org/10.3390/ma11101989
44. Ramachandran VS, Beaudoin JJ (2001) Handbook of Analytical Techniques in Concrete Science and Technology. William Andrew Publishing, New York
45. Bulou S, Brizoual LL, Miska P, Poucques LD, Hugon R, Belmahi M, Bougdira J (2011) The influence of CH_4 addition on composition, structure and optical characteristics of SiCN thin films deposited in a CH_4/N_2/Ar/hexamethyldisilazane microwave plasma. Thin Solid Films. https://doi.org/10.1016/j.tsf.2011.07.054
46. Hallam B, Tjahjono B, Wenham S (2012) Effect of PECVD silicon oxynitride film composition on the surface passivation of silicon wafers. Sol Energy Mater Sol C. https://doi.org/10.1016/j.solmat.2011.09.052
47. Ferreira I, Fortunato E, Vilarinho P, Viana AS, Ramos AR, Alves E, Martins R (2006) Hydrogenated silicon carbon nitride films obtained by HWCVD, PA-HWCVD and PECVD techniques. J Non-Cryst Solids. https://doi.org/10.1016/j.jnoncrysol.2006.02.025
48. Xiao X, Li Y, Song L, Peng X, Hu X (2006) Structural analysis and microstructural observation of SiC_xN_y films prepared by reactive sputtering of SiC in N_2 and Ar. Appl Surf Sci. https://doi.org/10.1016/S0169-4332(99)00493-6
49. Wrobel AM, Lezak IB, Uznanski P, Glebocki B (2010) Silicon Carbonitride (SiCN) Films by Remote Hydrogen Microwave Plasma CVD from Tris(dimethylamino)silane as Novel Single Source Precursor. Chem Vap Deposition. https://doi.org/10.1002/cvde.201004287
50. Guha S, Das S, Bandyopadhyay A, Das S, Swain BP (2018) Investigation of mechanical properties of CVD grown titanium silicon nitride thin films under reduced atmosphere. Appl Phys A. https://doi.org/10.1007/s00339-017-1455-7
51. Xiong K, Gu J (2015) Understanding pop-in phenomena in $FeNi_3$ nanoindentation. Intermetallics. https://doi.org/10.1016/j.intermet.2015.08.007
52. Ruffell S, Bradby JE, Williams JS, Munroe P (2007) Formation and growth of nanoindentation-induced high pressure phases in crystalline and amorphous silicon. J Appl Phys. https://doi.org/10.1063/1.2781394
53. Hu JZ, Merkle LD, Menoni CS, Spain IL (1986) Crystal data for high-pressure phases of silicon. Phys Rev B 34:4679. https://doi.org/10.1103/PhysRevB.34.4679
54. Oliver WC, Pharr GM (1992) An improved technique for determining hardness and elastic modulus using load and displacement sensing indentation experiments. J Mater Res. https://doi.org/10.1557/JMR.1992.1564
55. Hua G, Zhong J, Qi Y, Cheng X (2018) Influence of carbon on stability, mechanical property electronic structure and lattice dynamics of silicon carbonitride. J Am Ceram Soc. https://doi.org/10.1111/jace.15862
56. Ni W, Cheng YT, Lukitsch MJ, Weiner AM, Lev LC, Grummon DS (2004) Effects of the ratio of hardness to Young's modulus on the friction and wear behaviour of bilayer coatings. Appl Phys Lett. https://doi.org/10.1063/1.1811377

Publisher's Note Springer Nature remains neutral with regard to jurisdictional claims in published maps and institutional affiliations.